Two-Axis Solar Tracker Applied With All-Electric Ship

Nattapon Boonyapakdee[†], Non-member

ABSTRACT

The all-electric ship (AES) offers new hope for the reduction of fuel consumption and carbon emissions. To fully exploit the photovoltaics (PVs) installed on the AES, the two-axis solar tracker is proposed to find the best tilt and surface azimuth angles of PV panels. The tilt angle is computed by particle swarm optimization (PSO) regarding the time and ship location. The surface azimuth angle is adjusted according to the hemisphere. The dynamic performance of the proposed solar tracker is evaluated using MATLAB/Simulink simulation. According to the simulation results, the proposed solar tracker can obtain maximum energy all day, while the voyage time, fuel consumption, and carbon emissions are significantly reduced. Moreover, the proposed solar tracker can effectively operate under communication delay caused by the global positioning system (GPS).

Keywords: All-Electric Ships, AES, Solar Tracker, Communication Delays

LIST OF SYMBOLS

A_D and B_D	Coefficients of consumption curve
CML	Constant angle
FC	Fuel consumption
G_B	Beam radiation
G_{SC}	Solar constant
L_1 and L_2	Longitudes of consecutive locations
N	Number of the particles
P_i^k	Position
$P_{pbest,i}^k$	Personal best position
P_{gbest}	Global best position
P_{pro}	Propulsion load
P_N^D	Rated power of diesel generator
P_D	Output power of diesel generator
S_t	Current distance
S_{t-1}	Previous distance
V_t	Ship speed
a_1	Proportional coefficient
a_2	Exponential coefficient
c_1 and c_2	Acceleration coefficients
i	Subscript denoting order number of the particle
k	Superscript denoting the number of current iterations
k_{max}	Maximum number of iterations
n	Days
r_1 and r_2	Random values
v_i^k	Velocity
w	Inertia weight
β	Tilt angle
γ	Surface azimuth angle
ΔML	Distance between consecutive locations
Δt	Time step
δ	Declination
θ	Incidence angle
τ_B	Atmosphere transmittance
ϕ	Latitude
ϕ_1 and ϕ_2	Latitude of consecutive locations
ω	Hour angle

1. INTRODUCTION

The logistics of the marine industry are mainly carried out by shipboards due to the low cost, safety, and flexibility [1, 2]. Although maritime transport provides several benefits, it releases a large amount of greenhouse gas, equating to around 3–5% of global greenhouse gas emissions, while the fuel costs of ocean shipping are unpredictable [3, 4]. To improve the environmental impact, the international maritime organization (IMO) set the objective that all ships built after 2025 should reduce their carbon emission by 30% compared to 2005 [5]. Therefore, the aim of the all-electric ship (AES) is to achieve the IMO goal and avoid the unpredictability of rises in fuel costs.

The photovoltaic (PV) panels installed on the AES play an important role in reducing carbon emissions and fuel cost [6, 7]. Power management strategies are applied to effectively utilize the power generated from PV panels during the voyage. These are briefly reviewed as follows.

The rule-based method is applied with the power management strategies [8–11], using the predetermined state to control the power system. Although potentially

Manuscript received on August 5, 2021; revised on October 22, 2021; accepted on December 01, 2021. This paper was recommended by Associate Editor Kaan Kerdchuen.

The author is with the Department of Electrical Engineering, Faculty of Engineering at Sriracha, Kasetsart University Sriracha Campus, Thailand.

[†]Corresponding author: nattapon.b@eng.src.ku.ac.th

Digital Object Identifier: 10.37936/ecti-eec.2022202.246905

easy to implement, the performance of power management strategies may be degraded since the predetermined states can vary over time [12].

This problem can be avoided by introducing metaheuristic optimization into the power management strategies. In [13, 14], PSO is employed to minimize fuel consumption. To improve the effectiveness of power management strategies using fuzzy-based particle swarm optimization (FPSO), and adaptive multi-context cooperatively coevolving particle swarm optimization (AM-CCPSO) are applied [15, 16]. In addition to FPSO and AM-CCPSO, power strategies based on grey wolf optimization (GWO) are presented in [12]. The GWO can reduce operation costs in comparison to PSO [17]. The fuzzy logic-grey wolf (FL-GWO) is used with the power management strategy proposed in [18]. The FL-GWO can improve the calculation performance of conventional GWO.

Apart from the abovementioned strategies, the power management strategy proposed in [19] is interesting. The operation is divided into two stages. Both stages replace the DG output with PV power generation to reduce fuel consumption. Moreover, the speed of the AES is adjusted according to the power generated from the PV panels. If the PV generation increases, so does the speed of the AES.

However, the solar tracker of the AES has not been studied in previous literature. The solar tracker increases the amount of energy collected from the sun, enabling the AES to fully exploit the PV panels.

The contribution of this paper is twofold. First, a two-axis solar tracker of the AES is proposed to maximize the solar energy during the voyage by finding the best tilt and surface azimuth angles. The best tilt angle for PV panels is explored using PSO, while the surface azimuth angle is obtained by considering the hemisphere. Since maximum solar energy is collected from PV panels, the voyage time, fuel consumption, and carbon emissions can be reduced. Moreover, the proposed solar tracker will help to improve efficiency of the power management strategies because the PV power is increased. Second, the impact of communication delay caused by the use of GPS on the proposed solar tracker is investigated.

This paper is categorized into eight sections. The electrical system installed in the AES is reviewed in Section 2. Section 3 discusses the factors influencing the PV generation in the AES. The two-axis solar tracker for the AES is proposed in Section 4. Section 5 explains the mathematical model of the AES voyage. Section 6 describes the effect of delay caused by GPS navigation. The simulation results obtained from MATLAB/Simulink are presented in Section 7. Finally, the conclusions are stated in Section 8.

2. ELECTRICAL SYSTEM OF THE AES

The typical electrical power system of the AES is shown in Fig. 1. The electrical sources include the diesel generator (DG), PVs, and the battery delivering the power to service and propulsion loads via bus A or bus B [20].

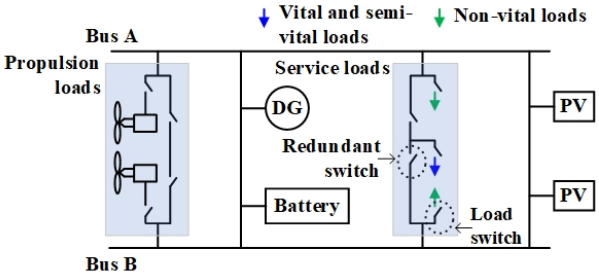

***Fig. 1**: Typical electrical system of the AES.*

The service loads are radar, navigation, lighting, and air conditioning. They can be classified into three types: vital load, semi-vital load, and non-vital load.

The load switch disconnects the non-vital load from the system during an emergency to prevent the occurrence of overload in the power source. The propulsion load is the electrical system driving the ship. Moreover, the redundant switch is applied to improve system reliability. For example, if bus A fails, bus B feeds the power to the service load and propulsion load via the redundant switch.

3. PVS INSTALLED ON THE AES

In recent years, PVs have been widely applied as shipboard power sources [21–23]. They can be installed on the deck and rooftop. For example, if the dimensions of an oil tanker are $332 \times 60 \times 30\,\mathrm{m}^3$, PV modules over $2000\,\mathrm{m}^2$ can be installed easily [24].

The electrical power system in the AES is comparable to a mobile microgrid. A mobile microgrid is quite different from the conventional microgrid because it cannot receive additional power from external sources such as utility [25, 26]. In the AES, if the PVs of the mobile microgrid cannot effectively harvest the energy from the sun, the voyage time and fuel consumption/carbon emissions will increase. Therefore, collecting energy from PVs is considered a serious issue for the AES.

The power generated by PVs mainly depends on the amount of beam radiation on the surface [27]. The controlling factors of PV panels affect the amount of beam radiation on the surface, including the tilt angle and surface azimuth angle as expressed in Eqs. (1) and (2), respectively [28, 29].

$$G_B = \tau_B G_{SC}\left[1 + 0.033\cos\frac{360n}{365}\right]\cos\theta \tag{1}$$

$$\begin{aligned}\cos\theta = {} & \sin\delta\sin\phi\cos\beta - \sin\delta\cos\phi\sin\beta\cos\gamma \\ & + \cos\delta\cos\phi\cos\beta\cos\omega + \cos\delta\sin\phi\cos\gamma\cos\omega \\ & + \cos\delta\sin\beta\sin\gamma\sin\omega\end{aligned} \tag{2}$$

Therefore, if the tilt angle and surface azimuth angle are properly adjusted, the beam radiation on the PV surface will be maximized. As can be observed from Fig. 2, the surface azimuth angle is between the projection of the

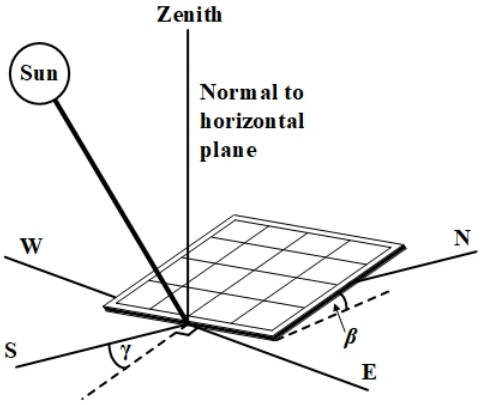

Fig. 2: Tilt angle and surface azimuth angle.

normal horizontal plane and local meridian. The tilt angle is between the PV panel and horizontal plane.

The declination and hour angle can be calculated as in the following equations [28].

$$\delta = 23.45 \sin\left(360 \frac{264 + n}{365}\right) \tag{3}$$

$$\omega = 15 \times (\text{solar time} - 12) \tag{4}$$

4. TWO-AXIS SOLAR TRACKER APPLIED USING THE AES

When the beam radiation on the surface of the PV panels is maximized, the maximum energy can be collected from the sun. The AES can fully utilize the PV panels. The two-axis solar tracker for the AES is therefore proposed to complete this objective. The PSO calculates the best tilt angle of the PV panels by considering time and ship location. The hemisphere is used to determine the surface azimuth angle.

As mentioned in [30, 31], the PSO is a simple method. Moreover, it is a powerful method since the PSO has a shorter calculation time and stable convergence compared to other methods [14]. This paper, therefore, chooses the PSO to search for the best tilt angle.

The PSO was developed by James Kennedy and Russell Eberhart in 1995. It is applied in many applications, such as autonomous navigation and PV applications [32, 33]. The PSO observes the movement of particles in space. Each particle moves with different velocity. The mathematical model of the PSO can be expressed by Eqs. (5) and (6) [34].

$$v_i^{k+1} = w \cdot v_i^k + c_1 \cdot r_1 \cdot (P_{pbest,i}^k - P_i^k) + c_2 \cdot r_2 \cdot (P_{gbest} - P_i^k) \tag{5}$$

$$P_i^{k+1} = P_i^k + v_i^{k+1};\ i = 1, 2, 3, \ldots, N;\ k = 1, 2, 3, \ldots, k_{max} \tag{6}$$

The algorithm flowchart of the PSO in the proposed solar tracker is shown in Fig. 3. The mathematical model expressed in Eqs. (5) and (6) is used to find the best tilt

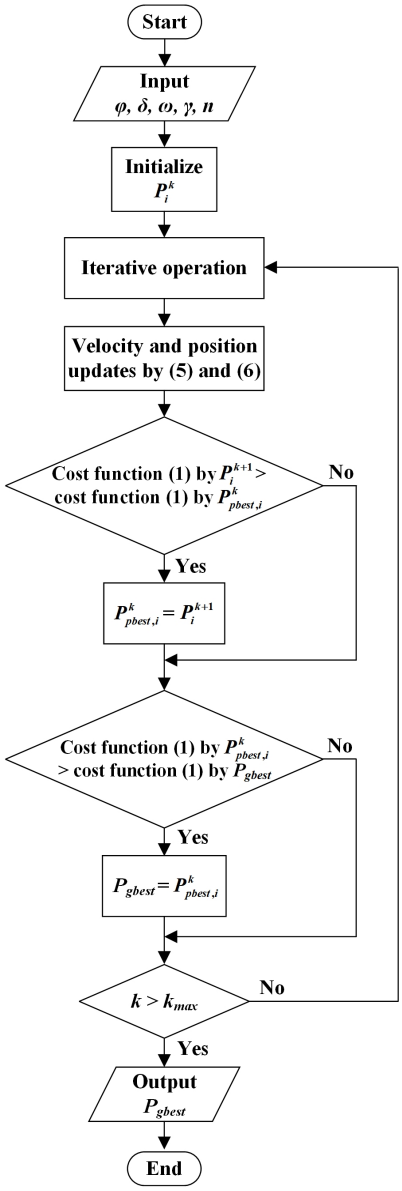

Fig. 3: Flowchart of particle swarm optimization programmed in the proposed solar tracker.

angle for the PV panels, and the position of the particles is represented by the tilt angle. The beam radiation in Eq. (1) is applied as the cost function of the PSO, while the declination and hour angle (time) of the cost function are computed by Eqs. (3) and (4), respectively.

The latitude (ship location) of the cost function is sent from the GPS navigation in the AES. The surface azimuth angle of the cost function is obtained by considering the hemisphere, as explained in the next paragraph. The latitude, declination, hour angle, surface azimuth angle, and days are set as the input. The position of particles is then represented by the tilt angle which is randomly initialized. In each iteration, the new velocity of each particle is calculated from the best personal and global positions, as shown in Eq. (5). The personal best position relates to each individual particle, while the global best

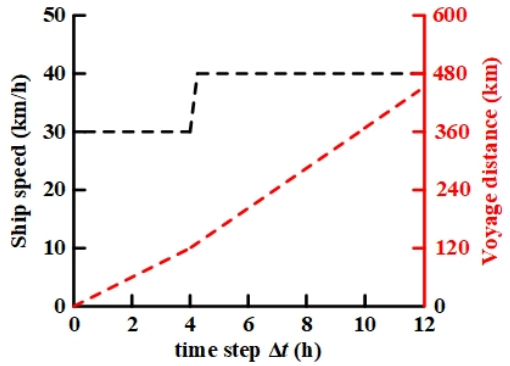

Fig. 4: Relationship between distance and speed.

position refers to the best position among all particles. The new position of each particle is updated by velocity, as shown in Eq. (6). The velocity moves the particles into the best position. The cost functions resulting from the new positions and personal best positions are then compared. If the cost functions resulting from the new positions are higher, these new positions are updated as the personal best positions. The cost functions resulting from the updated personal best positions and global best position are subsequently compared. If the cost function resulting from updated personal best position is greater, this personal best position is updated as the global best position. This loop occurs until the maximum number of iterations is achieved. In the final iteration, the global best position is set as the best tilt angle to achieve the maximum PV power.

The surface azimuth angle of the proposed solar tracker is obtained by considering the hemisphere [28]. It can be explained by Eqs. (7) and (8).

$$\gamma = 0^{\circ}; \qquad \text{for northern hemisphere} \tag{7}$$

$$\gamma = 180^{\circ}; \qquad \text{for southern hemisphere} \tag{8}$$

The hemisphere is defined by the latitude sent from the GPS navigation. If the latitude is positive, the northern hemisphere is indicated. The surface azimuth angle is then set at zero. Otherwise, the negative latitude implies the southern hemisphere. If the AES is located in the southern hemisphere, the surface azimuth angle is set at 180 degrees.

Finally, the best tilt angle and surface azimuth angle are sent to the controller of the motor control to adjust two axes of PV panels, and the PV power is maximized.

5. VOYAGE MODELING OF THE AES

This section describes the mathematical model introduced to simulate the cruise operation of the AES, including distance, latitude, longitude, and fuel consumption.

5.1 Distance

The distance is modeled by the accumulation of the product of ship speed and time step as shown in Fig. 4

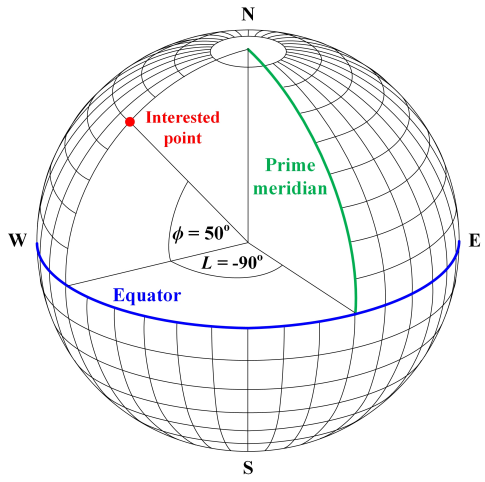

Fig. 5: Latitude and longitude measurements.

[19, 35]. It can be expressed as

$$S_t = S_{t-1} + V_t \cdot \Delta t \tag{9}$$

The ship speed is calculated according to the relationship between the electrical power consumed by the propulsion load and coefficients as in the following equation [36, 37].

$$V_t = \left(\frac{P_{pro}}{a_1}\right)^{\frac{1}{a_2}} \tag{10}$$

5.2 Latitude and Longitude

Locations on earth are commonly represented by latitude and longitude, the measurements of which are shown in Fig. 5. The latitude is the angle measured from the equator to the point of interest (positive for north and negative for south). The longitude is the angle measured from the prime meridian to the point of interest (positive for east and negative for west). The latitude and longitude of the AES are modeled using the mid-latitude formula [38]. By rearranging the equation for mid-latitude distance, the latitude can be expressed as

$$\phi_2 = \phi_1 + \frac{360}{40031.6} \cdot \Delta ML \cdot \cos(CML) \tag{11}$$

The equation for the mid-latitude course is rearranged to find the longitude. It can be expressed as follows.

$$L_2 = L_1 + \left[\frac{\tan(CML)}{\cos(\phi_M)} \cdot (\phi_2 - \phi_1)\right] \tag{12}$$

$$\phi_M = \frac{\phi_1 - \phi_2}{2} \tag{13}$$

In this paper, the latitude and longitude obtained from Eqs. (11) and (12) are assumed as the output of GPS navigation.

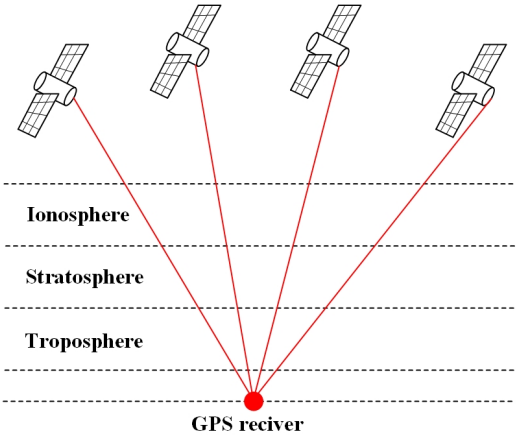

***Fig. 6**: Propagation of the GPS signal.*

5.3 Fuel Consumption

The fuel consumption of DGs can be modeled according to the output power [24, 39], and can be expressed as

$$FC = B_D \cdot P_N^D + A_D \cdot P_D \tag{14}$$

6. EFFECTS OF DELAY CAUSED BY USING GPS

Usually, the GPS is utilized to navigate vehicles, including cars, ships, and aircraft; however, the propagation delay between satellite and GPS receiver is considered to be a major problem. As shown in Fig. 6, the signal sent from the satellite to GPS receiver moves through multiple layers of the atmosphere. The free electrons and gases contained in the atmosphere cause the signal sent from the satellite to move slowly [40]. This propagation delay can affect the performance of some applications. For example, in [41], the position sent from the GPS is used in route calculation to avoid vehicle collision. If the position sent from the GPS contains some delays, an error occurs in the calculated route, causing an accident. Similarly, the proposed solar tracker uses the data sent from the GPS in tilt angle and surface azimuth angle calculations. Therefore, the effect of a communication delay on the proposed solar tracker needs to be investigated.

7. SIMULATION ASSESSMENT

The MATLAB/Simulink simulation is utilized to evaluate the performance of the proposed solar tracker. To simplify the evaluation process, the AES load only consists of 4 MW of electric propulsion loads. The rating of the DGs must be designed to ensure sufficient propulsion loads [37]. The 4.5 MW of the DGs and the 2 MW of the PVs are installed on the AES. The simulation assessment is divided into five cases, the parameters of which are the same, as shown in Table 1.

The first case validates the effectiveness of the proposed solar tracker using statistical calculation. The ship is located at Port Miami (United States) on April 30. The

***Table 1**: Parameters in simulation.*

Radiation model	G_{SC}	1367 W/m^2
	τ_B	0.8
PSO	c_1	2
	c_2	2
	w	0.5
	r_1	[0, 1]
	r_2	[0, 1]
	N	100
	k_{max}	100
Propulsion load model	a_1	20
	a_2	3
Fuel consumption model	P_N^D	4.5 MW
	B_D	0.0845 L/h
	A_D	0.246 L/h

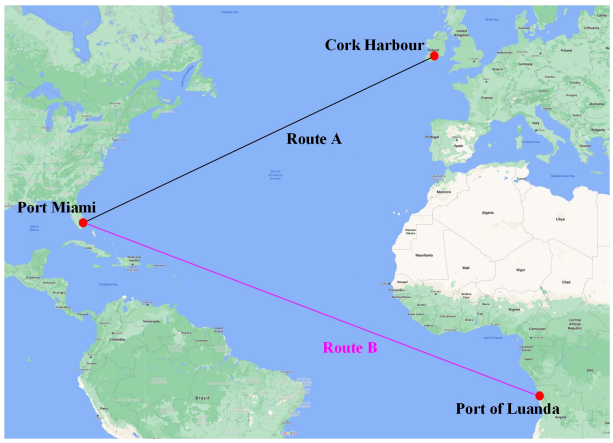

***Fig. 7**: Route map used in simulation.*

second and third cases examine the voyage time and fuel consumption/carbon emissions, respectively. The route map is illustrated in Fig. 7. On April 30, the AES starts its voyage from Port Miami to Cork Harbour (Ireland) through route A. The distance between the two locations is 6327 km. The fourth case is set to verify the performance of the proposed solar tracker when the AES voyages from the northern hemisphere to the southern hemisphere through route B. The AES started to move from Port Miami to the Port of Luanda (Angola) on April 30. The distance between the two locations is 10 767 km. In the fifth case, the performance of the proposed solar tracker under the delay caused by the use of GPS navigation is investigated. The delay from GPS navigation is set at 2 s [42]. The voyage schedule is the same as in the second and third cases.

In the first case, the relationship between the tilt angle and iterations is shown in Fig. 8. The proposed solar tracker calculates the best tilt angle as 0.157937 degrees within 20 iterations. This value is equal to the best tilt angle obtained from the numerical method. The mean and standard deviation are 0.157794 and 2.85×10^{-3} degrees, respectively. Therefore, the speed and accuracy

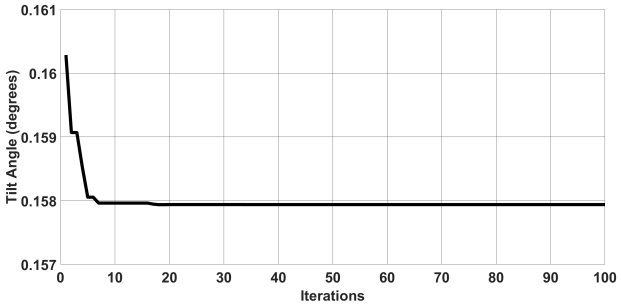

***Fig. 8**: Relationship between tilt angle and iterations.*

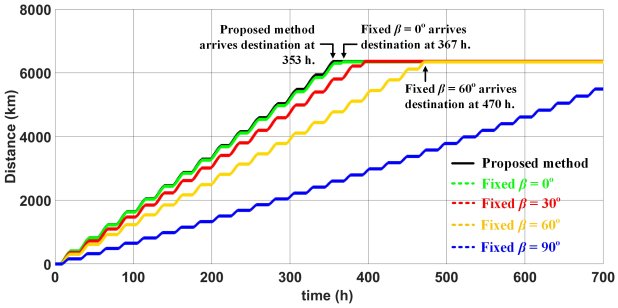

***Fig. 11**: Voyage distance in the second case.*

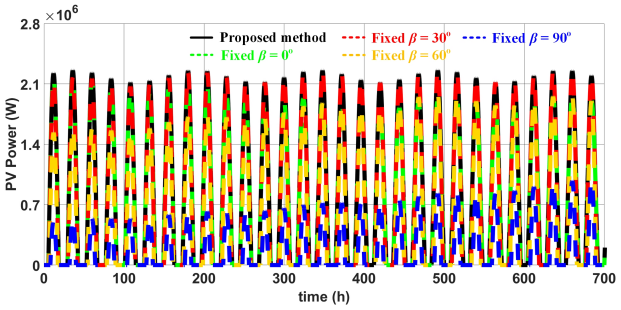

***Fig. 9**: PV power in the second case.*

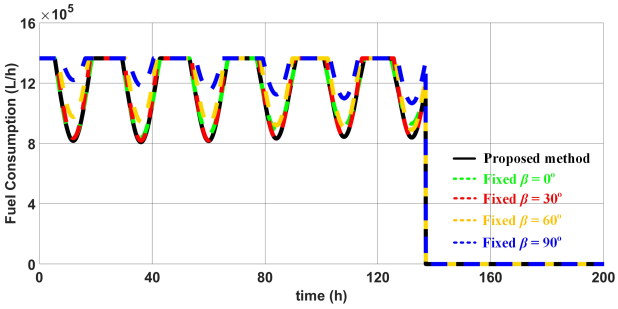

***Fig. 12**: Fuel consumption in the third case.*

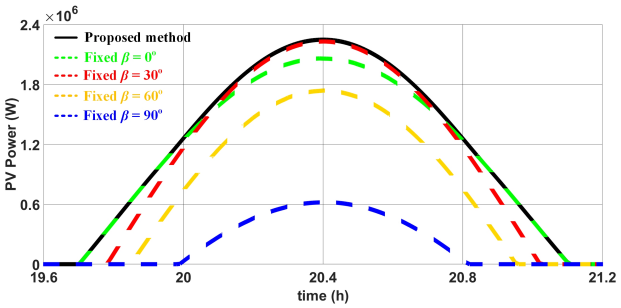

***Fig. 10**: Magnified PV power in the second case.*

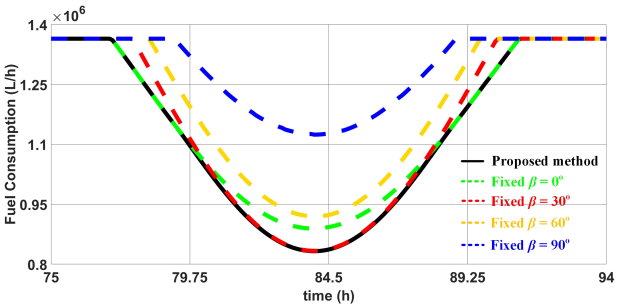

***Fig. 13**: Magnified fuel consumption in the third case.*

calculations for the proposed solar tracker are satisfied.

To clearly show the benefit of the proposed solar tracker for the AES voyage time, the electric propulsion loads receive power only from the PV panels. During the voyage, the surface azimuth angle provided by the proposed solar tracker is zero since Port Miami and Cork Harbour are in the northern hemisphere. The power generated by the PVs is shown in Fig. 9. The PV power between 19.6 and 21.2 hours is magnified in Fig. 10. The power generated based on the proposed solar tracker is higher than that for the fixed tilt angles and fixed surface azimuth angle at zero. As shown in Fig. 11, the AES using the proposed solar tracker reaches Cork Harbour in the fastest time. It is approximately 14 hours faster when comparing zero degrees of the tilt angle. Therefore, the proposed solar tracker can reduce the voyage time. This would be significantly advantageous to a power management strategy that adjusts the ship speed according to the PV power [19].

In the third case, the PVs and DGs feed the power into the electric propulsion loads. When the PV power is insufficient, it is supported by the DGs. The fuel consumption of the DGs during the voyage is shown in Fig. 12 and magnified over 75 and 94 hours as shown in Fig. 13. As can be observed from Fig. 13, the proposed solar tracker consumes the least amount of fuel. This is because the AES generates the maximum PV power. In addition, the AES under the proposed solar tracker provides the greatest reduction in carbon emissions, as shown in Fig. 14. Hence, the proposed solar tracker can improve fuel consumption and mitigate the environmental problems caused by maritime transport.

In the fourth case, since the AES voyages from the northern to the southern hemisphere, the surface azimuth angle is adjusted to zero or 180 degrees by the proposed solar tracker. As shown in Fig. 15, the proposed solar tracker still gives the greatest PV power during the voyages. Therefore, the proposed solar tracker can work in both hemispheres.

In the fifth case, delay is introduced into the output

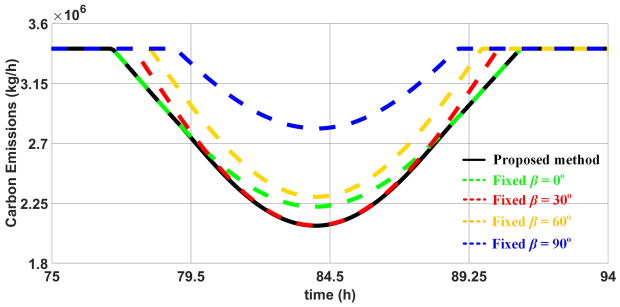

***Fig. 14**: Magnified carbon emissions in the third case.*

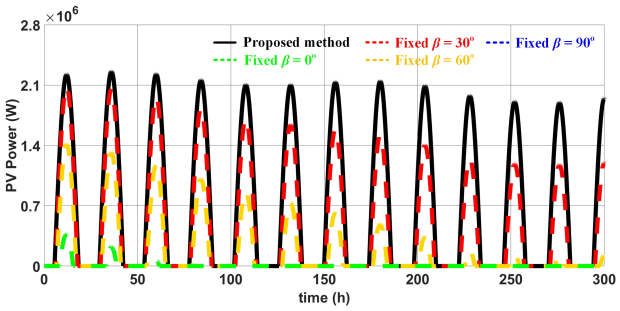

***Fig. 15**: PV power in the fourth case.*

of GPS navigation. As shown in Fig. 16, the proposed solar tracker with 2 s of GPS signal delay can provide the PV power as in the case without GPS signal delay. Consequently, the proposed solar tracker can operate effectively, although the output of the GPS signal has some delays.

These simulation results demonstrate the performance of the proposed solar tracker. It can maximize the power generated from the PV panels and increase the PV power by around 7.5% when compared with the fixed tilt angle at zero. Consequently, in the voyage time, fuel consumption and carbon emissions are reduced significantly. However, the swing motion affecting the PV power is neglected in this paper and will be further studied in future work. Moreover, the proposed solar tracker can correctly operate, although the AES travels between the northern and southern hemispheres. It is therefore clear that the PV power can be maximized at any time of day and at any location. In the event of some delay in the output of GPS navigation, the proposed solar tracker can still operate satisfactorily, since the power generated by the PV panels is still maximized.

8. CONCLUSION

This paper proposes a two-axis solar tracker for the AES to maximize PV power. The tilt angle is calculated by PSO, taking the time and ship location into account. The surface azimuth angle is adjusted depending on the latitude of the AES. The effectiveness of the proposed solar tracker is validated through simulation. The results show that the proposed solar tracker offers the maximum PV power during any voyage. Therefore, the voyage

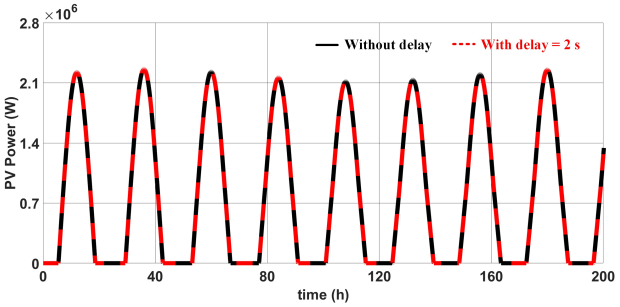

***Fig. 16**: PV power in the fifth case.*

time and fuel consumption/carbon emissions can be significantly reduced. In the event of a communication delay caused by GPS navigation, the proposed solar tracker can operate without any problems.

REFERENCES

[1] D. Naletina and E. Perkov, "The economic importance of maritime shipping with special reference on Croatia," in *Proceeding of 19th International Scientific Conference on Economic and Social*, Melbourne, Australia, 2017.

[2] D. Richardson, N. Castree, M. F. Goodchild, A. Kobayashi, W. Liu, and R. A. Marston, Eds., *The International Encyclopedia of Geography*. New York, USA: John Wiley & Sons, 2017.

[3] M. M. Rahim, M. T. Islam, and S. Kuruppu, "Regulating global shipping corporations' accountability for reducing greenhouse gas emissions in the seas," *Marine Policy*, vol. 69, pp. 159–170, Jul. 2016.

[4] S. Fang, Y. Xu, Z. Li, Z. Ding, L. Liu, and H. Wang, "Optimal sizing of shipboard carbon capture system for maritime greenhouse emission control," *IEEE Transactions on Industry Applications*, vol. 55, no. 6, pp. 5543–5553, Nov. 2019.

[5] *Revised MARPOL Annex VI: Regulations for the Prevention of Air Pollution from Ships and NOx Technical Code*. London, UK: International Maritime Organization, 2008.

[6] A. Kurniawan and E. Shintaku, "Control of photovoltaic system connected to DC bus in all-electric ship," in *2017 International Conference on Advanced Mechatronics, Intelligent Manufacture, and Industrial Automation (ICAMIMIA)*, 2017, pp. 110–115.

[7] A. Accetta and M. Pucci, "Energy management system in DC micro-grids of smart ships: Main gen-set fuel consumption minimization and fault compensation," *IEEE Transactions on Industry Applications*, vol. 55, no. 3, pp. 3097–3113, May 2019.

[8] J. Han, J.-F. Charpentier, and T. Tang, "An energy management system of a fuel cell/battery hybrid boat," *Energies*, vol. 7, no. 5, pp. 2799–2820, 2014.

[9] A. M. Bassam, A. B. Phillips, S. R. Turnock, and P. A. Wilson, "An improved energy management strategy for a hybrid fuel cell/battery passenger

vessel," *International Journal of Hydrogen Energy*, vol. 41, no. 47, pp. 22 453–22 464, Dec. 2016.

[10] A. M. Bassam, A. B. Phillips, S. R. Turnock, and P. A. Wilson, "Development of a multi-scheme energy management strategy for a hybrid fuel cell driven passenger ship," *International Journal of Hydrogen Energy*, vol. 42, no. 1, pp. 623–635, Jan. 2017.

[11] M. Kalikatzarakis, R. Geertsma, E. Boonen, K. Visser, and R. Negenborn, "Ship energy management for hybrid propulsion and power supply with shore charging," *Control Engineering Practice*, vol. 76, pp. 133–154, Jul. 2018.

[12] M. D. Al-Falahi, K. S. Nimma, S. D. Jayasinghe, H. Enshaei, and J. M. Guerrero, "Power management optimization of hybrid power systems in electric ferries," *Energy Conversion and Management*, vol. 172, pp. 50–66, Sep. 2018.

[13] E. A. Sciberras, B. Zahawi, D. J. Atkinson, A. Breijs, and J. H. van Vugt, "Managing shipboard energy: A stochastic approach special issue on marine systems electrification," *IEEE Transactions on Transportation Electrification*, vol. 2, no. 4, pp. 538–546, Dec. 2016.

[14] S. Paran, T. V. Vu, T. E. Mezyani, and C. S. Edrington, "MPC-based power management in the shipboard power system," in *2015 IEEE Electric Ship Technologies Symposium (ESTS)*, 2015, pp. 14–18.

[15] F. D. Kanellos, A. Anvari-Moghaddam, and J. M. Guerrero, "A cost-effective and emission-aware power management system for ships with integrated full electric propulsion," *Electric Power Systems Research*, vol. 150, pp. 63–75, Sep. 2017.

[16] R. Tang, X. Li, and J. Lai, "A novel optimal energy-management strategy for a maritime hybrid energy system based on large-scale global optimization," *Applied Energy*, vol. 228, pp. 254–264, Oct. 2018.

[17] K. Nimma, M. Al-Falahi, H. D. Nguyen, S. D. G. Jayasinghe, T. Mahmoud, and M. Negnevitsky, "Grey wolf optimization-based optimum energy-management and battery-sizing method for grid-connected microgrids," *Energies*, vol. 11, no. 4, 2018, Art. no. 847.

[18] M. D. Al-Falahi, S. D. Jayasinghe, and H. Enshaei, "Hybrid algorithm for optimal operation of hybrid energy systems in electric ferries," *Energy*, vol. 187, Nov. 2019, Art. no. 115923.

[19] S. Fang, Y. Xu, S. Wen, T. Zhao, H. Wang, and L. Liu, "Data-driven robust coordination of generation and demand-side in photovoltaic integrated all-electric ship microgrids," *IEEE Transactions on Power Systems*, vol. 35, no. 3, pp. 1783–1795, May 2020.

[20] Q. Xu, B. Yang, Q. Han, Y. Yuan, C. Chen, and X. Guan, "Optimal power management for failure mode of MVDC microgrids in all-electric ships," *IEEE Transactions on Power Systems*, vol. 34, no. 2, pp. 1054–1067, Mar. 2019.

[21] B. Zahedi and L. E. Norum, "Modeling and simulation of all-electric ships with low-voltage DC hybrid power systems," *IEEE Transactions on Power Electronics*, vol. 28, no. 10, pp. 4525–4537, Oct. 2013.

[22] S. Fang, Y. Wang, B. Gou, and Y. Xu, "Toward future green maritime transportation: An overview of seaport microgrids and all-electric ships," *IEEE Transactions on Vehicular Technology*, vol. 69, no. 1, pp. 207–219, Jan. 2020.

[23] M. A. Igder, M. Rafiei, J. Boudjadar, and M.-H. Khooban, "Reliability and safety improvement of emission-free ships: Systemic reliability-centered maintenance," *IEEE Transactions on Transportation Electrification*, vol. 7, no. 1, pp. 256–266, Mar. 2021.

[24] S. Wen, H. Lan, Y.-Y. Hong, D. C. Yu, L. Zhang, and P. Cheng, "Allocation of ESS by interval optimization method considering impact of ship swinging on hybrid PV/diesel ship power system," *Applied Energy*, vol. 175, pp. 158–167, Aug. 2016.

[25] S. Fang, B. Gou, Y. Wang, Y. Xu, C. Shang, and H. Wang, "Optimal hierarchical management of shipboard multibattery energy storage system using a data-driven degradation model," *IEEE Transactions on Transportation Electrification*, vol. 5, no. 4, pp. 1306–1318, Dec. 2019.

[26] S. Wen, T. Zhao, Y. Tang, Y. Xu, M. Zhu, and Y. Huang, "A joint photovoltaic-dependent navigation routing and energy storage system sizing scheme for more efficient all-electric ships," *IEEE Transactions on Transportation Electrification*, vol. 6, no. 3, pp. 1279–1289, Sep. 2020.

[27] Z. Zhen *et al.*, "The effects of inclined angle modification and diffuse radiation on the sun-tracking photovoltaic system," *IEEE Journal of Photovoltaics*, vol. 7, no. 5, pp. 1410–1415, Sep. 2017.

[28] J. A. Duffie and W. A. Beckman, *Solar Engineering of Thermal Processes*, 4th ed. New York, USA: John Wiley & Sons, 2013.

[29] C. Stanciu and D. Stanciu, "Optimum tilt angle for flat plate collectors all over the world – a declination dependence formula and comparisons of three solar radiation models," *Energy Conversion and Management*, vol. 81, pp. 133–143, May 2014.

[30] A. Wesabi Ibrahim *et al.*, "PV maximum power-point tracking using modified particle swarm optimization under partial shading conditions," *Chinese Journal of Electrical Engineering*, vol. 6, no. 4, pp. 106–121, Dec. 2020.

[31] Q. Zhao and C. Li, "Two-stage multi-swarm particle swarm optimizer for unconstrained and constrained global optimization," *IEEE Access*, vol. 8, pp. 124 905–124 927, Jul. 2020.

[32] S. Biswas, S. G. Anavatti, and M. A. Garratt, "A particle swarm optimization based path planning method for autonomous systems in unknown terrain," in *2019 IEEE International Conference on Industry 4.0, Artificial Intelligence, and Communications Technology (IAICT)*, 2019, pp. 57–63.

[33] R. B. A. Koad, A. F. Zobaa, and A. El-Shahat, "A novel MPPT algorithm based on particle swarm

optimization for photovoltaic systems," *IEEE Transactions on Sustainable Energy*, vol. 8, no. 2, pp. 468–476, Apr. 2017.

[34] M. Clerc, *Particle Swarm Optimization*. London, UK: ISTE, 2006.

[35] Z. Li, Y. Xu, S. Fang, X. Zheng, and X. Feng, "Robust coordination of a hybrid AC/DC multi-energy ship microgrid with flexible voyage and thermal loads," *IEEE Transactions on Smart Grid*, vol. 11, no. 4, pp. 2782–2793, Jul. 2020.

[36] F. D. Kanellos, "Optimal power management with GHG emissions limitation in all-electric ship power systems comprising energy storage systems," *IEEE Transactions on Power Systems*, vol. 29, no. 1, pp. 330–339, Jan. 2014.

[37] C. Shang, D. Srinivasan, and T. Reindl, "Economic and environmental generation and voyage scheduling of all-electric ships," *IEEE Transactions on Power Systems*, vol. 31, no. 5, pp. 4087–4096, Sep. 2016.

[38] H. Umland, "A short guide to celestial navigation." [Online]. Available: https://celnav.de/

[39] H. Lan, S. Wen, Y.-Y. Hong, D. C. Yu, and L. Zhang, "Optimal sizing of hybrid PV/diesel/battery in ship power system," *Applied Energy*, vol. 158, pp. 26–34, Nov. 2015.

[40] A. Hornbostel, "Propagation problems in satellite navigation," *URSI Radio Science Bulletin*, vol. 2009, no. 329, pp. 21–30, Jun. 2009.

[41] L. Bowen and Y. Danya, "Calculation of vehicle real-time position overcoming the GPS positioning latency with MEMS INS," in *Proceedings of 2014 IEEE International Conference on Service Operations and Logistics, and Informatics (SOLI)*, 2014, pp. 248–254.

[42] R. B. Langley, "RTK GPS," *GPS World*, vol. 9, no. 9, pp. 70–76, Sep. 1998.

Nattapon Boonyapakdee received his B.Eng., M.Eng., and D.Eng. degrees from King Mongkut's University of Technology Thonburi (KMUTT), Bangkok, Thailand, in 2011, 2014 and 2020, respectively. Recently, he is a Lecturer in Department of Electrical Engineering, Kasetsart University Sriracha Campus, Thailand. His research interests include smart grid, microgrid, control of distributed generators, and real-time applications.